

# Recent measurements in the beauty, charm, and tau sectors at Belle II

N.K.Rad<sup>a</sup>

*Deutsches Elektronen-Synchrotron,  
22607 Hamburg, Germany  
navid.khandan.rad@desy.de*

The first  $e^+e^-$  collisions at SuperKEKB took place in the early 2019, and since then more than  $100 \text{ fb}^{-1}$  of data have been collected by the Belle II detector. Although, for many measurements, the collected data is still not large enough to compete with previous measurements at Belle and BaBar, the improvements in the detector and analysis techniques have allowed many measurements to be already competitive in terms of systematic uncertainties. This document will briefly summarize some of the recent preliminary measurements in the beauty, charm and tau sectors at the Belle II.

## 1 Introduction

SuperKEKB<sup>1</sup> is an energy asymmetric  $e^+e^-$  collider, located in Tsukuba, Japan and is operating at nominal center-of-mass energy of 10.58 GeV, near the mass of  $\Upsilon(4S)$  resonance. The peak instantaneous luminosity of the machine is expected to reach 30 times that of its predecessor, which will make it possible the Belle II<sup>2</sup> detector to collect up to  $50 \text{ ab}^{-1}$  of collision data in its lifetime. In addition to being well known as a 2nd generation B-factory, the Belle II detector is a charm and tau factory as well since around a billion b, c, and  $\tau$  pair events are expected to be produced in every  $\text{ab}^{-1}$  of collected data by the experiment.

## 2 Results towards inclusive and exclusive measurements of $V_{cb}$

Precision measurements of Cabibbo–Kobayashi–Maskawa (CKM) matrix parameters are one of the main goals of the Belle II detector. In particular, studying the semileptonic decays of B-mesons has been the leading method for  $V_{cb}$  measurement. There has been, however, a long-standing tension between the inclusive and exclusive measurements of these decay modes and the upcoming measurements at Belle II are expected to improve the precision in both inclusive and exclusive measurements. An exclusive measurement of the branching fraction of  $B^0 \rightarrow D^{*-} \ell^+ \nu$  decay mode<sup>3</sup> has already been performed using  $34.6 \text{ fb}^{-1}$  of data. However, currently, these measurements are limited by the uncertainties arising from the reconstruction efficiencies of the slow-pions. These uncertainties are expected to decrease as larger control samples are collected for further investigations. Using, the same dataset, the hadronic mass moments have also been measured in  $B \rightarrow X_c \ell \nu$  channel<sup>4</sup>, where  $X_c$  represents the charm system. Moreover, an alternative method for measuring  $V_{cb}$  using the  $q^2$  moments is also currently in progress at Belle II and expected to become public soon.

---

<sup>a</sup>On behalf of the Belle II Collaboration.

### 29 3 Measurement of the time-integrated mixing probability $\chi_d$

30 The goal of this analysis<sup>5</sup> is to measure the time-integrated mixing probability  $\chi_d$ , which can  
 31 be used to set constraints on the mixing parameters of the neutral B-mesons. For this measure-  
 32 ments, both reconstructed B-mesons in the event are required to decay semi-leptonically and  
 33 the flavor of each B-meson is then inferred from the charge of its daughter lepton. By using  
 34 the number of same-sign ( $N_{SS}$ ) and opposite-sign ( $N_{OS}$ ) BB events, the  $\chi_d$  parameter can be  
 35 calculated as:

$$\chi_d = \frac{N_{SS}}{N_{SS} + N_{OS} \cdot (\epsilon_{OS}/\epsilon_{SS})^{-1}} \cdot (1 + r_B), \quad (1)$$

36 where  $r_B$  is a correction factor taking into account the contribution from the semi-leptonic decays  
 37 of charged B mesons and  $\epsilon_{OS}$  ( $\epsilon_{SS}$ ) is the selection efficiencies for the opposite-sign (same-sign)  
 38 modes and is measured using signal MC samples. In this analysis only the electron channel  
 39 is used where the electrons are required to momentum of at least 1 GeV in the center-of-mass  
 40 frame and must also also pass a tight electron identification likelihood. The signal yields in each  
 41 channel are extracted after fitting the sum of magnitudes of the electron momenta ( $p_{ee}$ ) to data.  
 42 Using the post-fit distributions shown in Fig. 3,  $\chi_d$  is measured as:

$$\chi_d = 0.187 \pm 0.010 \text{ (stat.)} \pm 0.019 \text{ (syst.)}, \quad (2)$$

43 where the dominating source of systematic is due to the corrections for electron identification.  
 44 However, these corrections are expected to improve as larger control samples are obtained. The  
 45 measured value of  $\chi_d$  is compatible with the world-average value and has a competitive precision  
 46 compared to the world average of time-independent measurements.

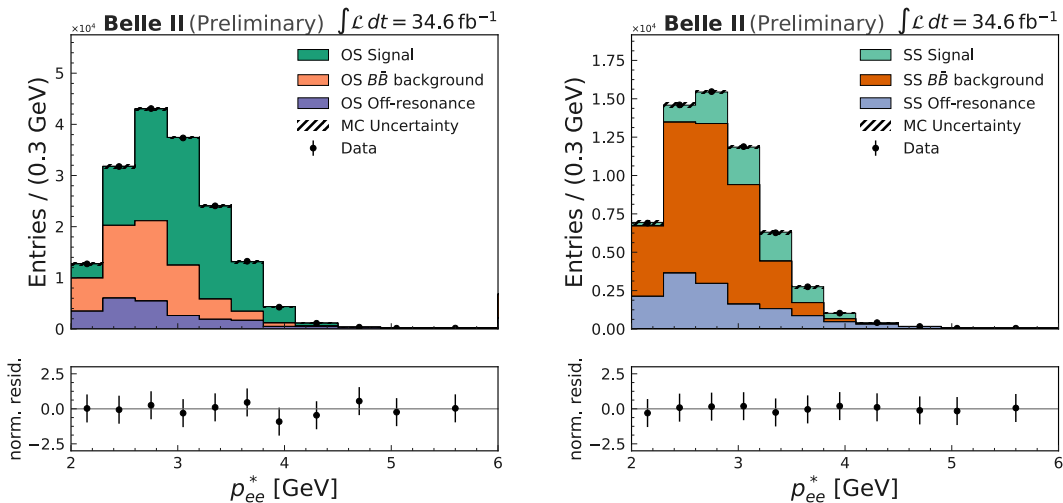


Figure 1 – The  $p_{ee}$  post-fit distributions for the opposite-sign (left) and same-sign (right) channels are shown. The lower plots show the pull between the data and the fit results, including the statistical uncertainty in data and the total uncertainty in the MC.

### 47 4 Rediscovery of the $B \rightarrow \eta' K$

48 The decay of the B meson into  $\eta' K$  is a charmless hadronic decay, mediated via hadronic penguin  
 49 diagrams which are also sensitive to the contributions of possible new physics in the hadronic  
 50 loop. Although this is a rare decay mode, the branching fraction is large enough to make time-  
 51 dependent measurements of CP violation parameters in this channel possible. The rediscovery<sup>6</sup>  
 52 of this decay mode at Belle II marks an important step towards improving these measurements.

53 For the reconstruction of the signal decay mode, both neutral and charged B mesons are  
 54 used, and for the decay modes of  $\eta'$ ,  $\eta' \rightarrow \eta(\rightarrow \gamma\gamma)\pi^+\pi^-$  and  $\eta' \rightarrow \rho(\rightarrow \pi^+\pi^-)\gamma$  are used. The  
 55 background processes contributing to this measurement are mostly due to continuum events,  
 56 but there is also non-negligible contamination due to misreconstructed signal events, referred  
 57 to as signal-cross-feed or SxF. In order to suppress the continuum backgrounds, a dedicated  
 58 multivariate classifier,  $CS_{var}$ , is trained on event shape variables such as Fox-Wolfram moments  
 59 and CLEO cones. The performance of this variable is validated by comparing the output in  
 60 simulation and the off-resonance dataset and assigning the differences as a source systematic  
 61 uncertainty.

62 In order to extract the signal yields, an extended unbinned three-dimensional maximum  
 63 likelihood fit is used. The three observables used in the fit are  $M_{bc}$ ,  $\Delta E$  and the continuum  
 64 suppression variable ( $CS_{var}$ ) and three components of the fit include signal, continuum and  
 65 peaking backgrounds. The contribution due to signal-cross-feed is considered together with  
 66 the signal component. The PDF used for modeling each contribution in each observable was  
 67 determined based on the MC. The fit process was also validated using toy MC with injected  
 68 signals. Figure 2 shows the result of the fit in each of the observables. The measurement of the  
 69 branching fraction and comparison to the world average are shown in Table 1.

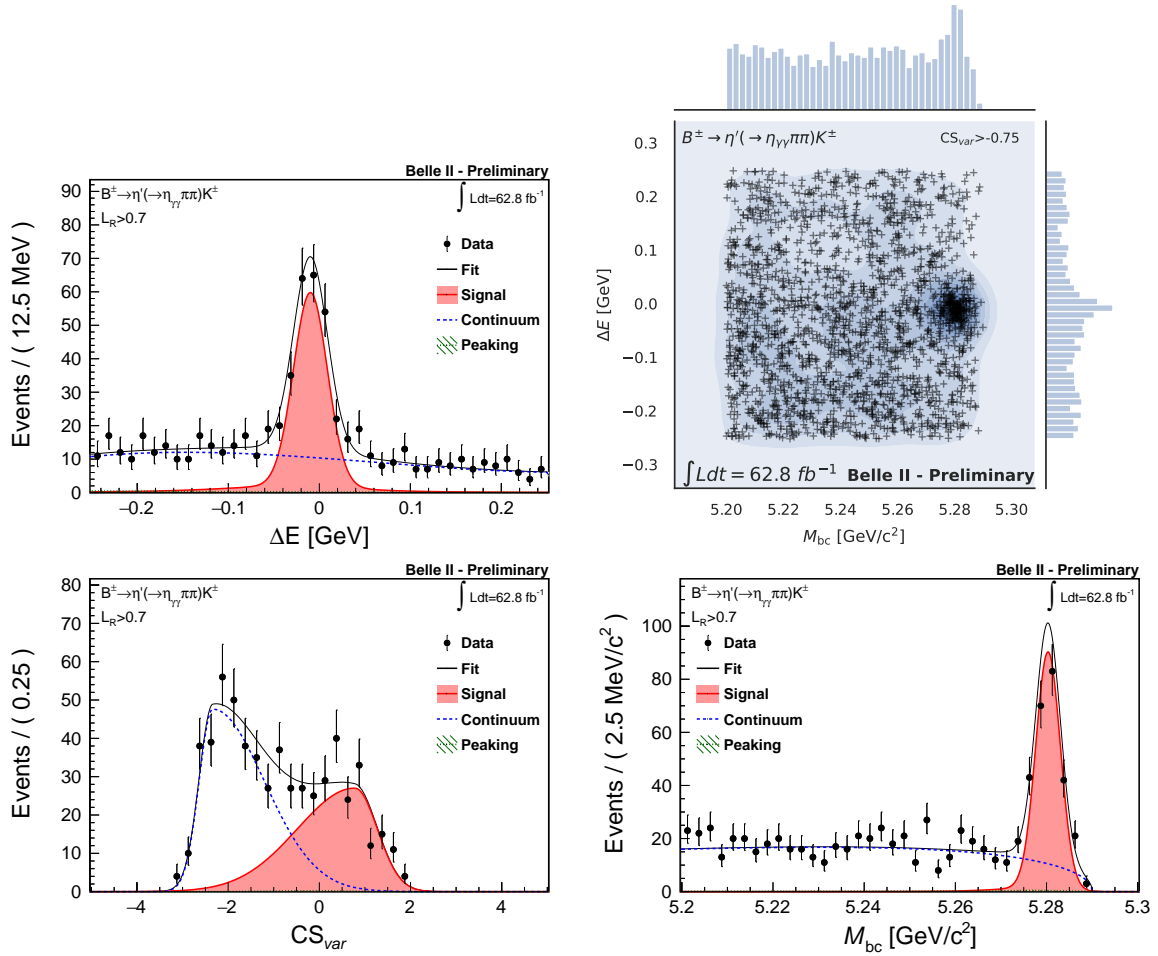


Figure 2 – Data and MC distributions and the corresponding fit results of  $M_{bc}$  and  $\Delta E$ , and  $CS_{var}$  in the channel  $B^{\pm} \rightarrow \eta' K^{\pm}$  with  $\eta' \rightarrow \eta\pi^+\pi^-$  are shown. Additionally the plot of  $M_{bc}$  versus  $\Delta E$  in the same channel are also shown.

Table 1: Summary of the results on the branching ratios of  $B \rightarrow \eta' K$  obtained by Belle II and the comparison with world averages.

Channel	$\mathcal{B} (\times 10^6)$	
	Belle II ( $62.8 \text{ fb}^{-1}$ )	World average
$B^\pm \rightarrow \eta' K$	$63.4^{+3.4}_{-3.3}(\text{stat}) \pm 3.4(\text{syst})$	$70.4 \pm 2.5$
$B^0 \rightarrow \eta' K^0$	$59.9^{+5.8}_{-5.5}(\text{stat}) \pm 2.7(\text{syst})$	$66 \pm 4$

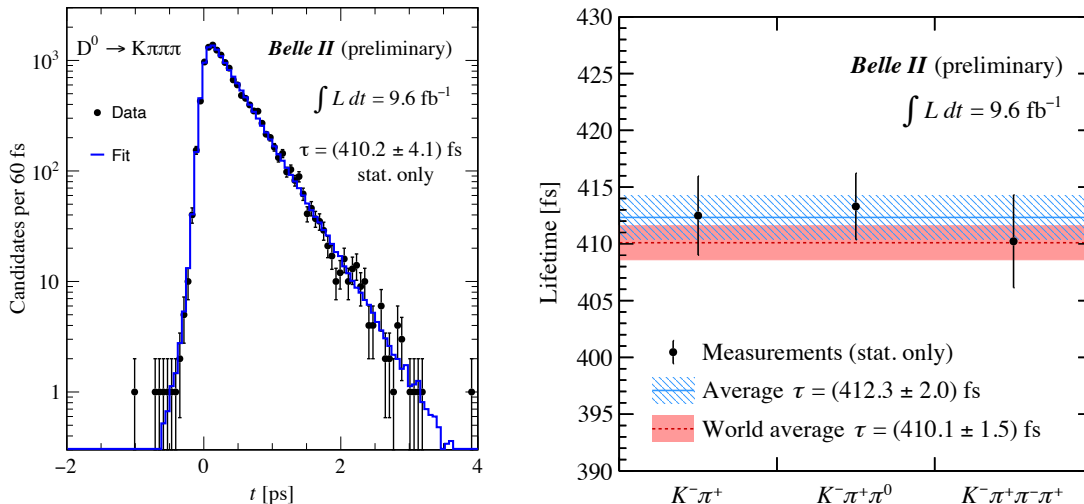


Figure 3 – The left plot shows the fit of the proper-time distribution of the  $D^*$ -tagged candidates in the  $D^0 \rightarrow K^- \pi^+$  channel. The right plot shows the comparison of the  $D^0$  measurements at Belle II and their comparison to the world average values.

## 70 5 $D^0$ lifetime measurement

71 For this preliminary measurement of the  $D^0$  lifetime in  $9.6 \text{ fb}^{-1}$  of Belle II data,  $D^{*+} \rightarrow D^0 \pi_s^+$   
72 candidates are used, in which the  $D^0$  decays to  $K^- \pi^+$ ,  $K^- \pi^+ \pi^0$ , or  $K^- \pi^+ \pi^+ \pi^-$ . Here,  $\pi_s^+$  refers  
73 to a soft-pion which due to the small mass difference between the  $D^*$  and  $D^0$ , has a relatively  
74 small momentum. In order to avoid any bias due to the non-zero lifetime of the B-meson,  $D^*$   
75 candidates from a B-meson are vetoed by requiring their momentum in the center-of-mass frame  
76 to be larger than  $2.5 \text{ GeV}$ . The  $D^0$  decay time and decay-time uncertainty are determined from  
77 the vertex fits of the production and decay vertices. The decay vertex is fitted using the  $K$   
78 and  $\pi$  candidates, and for the production vertex the measured position of the beams interaction  
79 point is also used as an additional constraint. As seen in Fig. 3, the measurements in the three  
80 channels are compatible with each other and with the world-average value within the statistical  
81 uncertainties. An updated measurement of the  $D^0$  and  $D^+$  lifetimes, using  $72 \text{ fb}^{-1}$  of data, with  
82 a precision competitive to the world-average values is expected to become public soon.

## 83 6 Yield extraction of $D^{*+} \rightarrow D^0(\pi^+ \pi^- \pi^0) \pi^+$

84 The large number of the charm sample which is expected to be collected at Belle II in the coming  
85 years, will allow for in depth investigations into CP violation (CPV) in the charm sector as well.  
86 In particular, the time-integrated Dalitz analysis of  $D^0(\pi^+ \pi^- \pi^0)$  mode could be used to search  
87 for CPV in the decay of  $D^0$ . As a step towards such a measurement, the current dataset is used  
88 to demonstrate the ability of the experiment to extract the yield for the signal candidates. The  
89 signal yield is extracted using the distribution  $\Delta M$ , where  $\Delta M = m(D^*) - m(D^0)$ . Figure 4  
90 shows the result of the fit on data corresponding to an integrated luminosity of  $72 \text{ fb}^{-1}$ . The

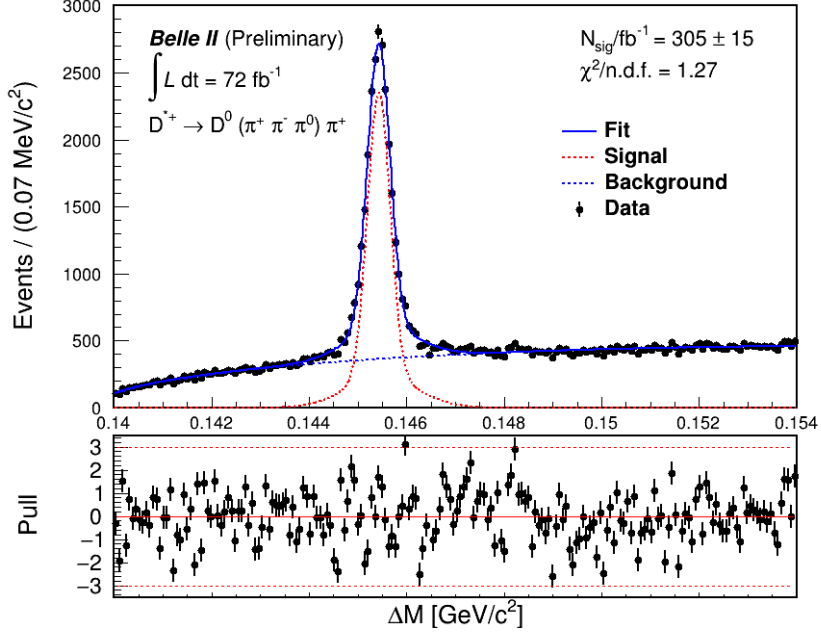


Figure 4 – The distribution of  $\Delta M$  in the  $D^{*+} \rightarrow D^0(\pi^+\pi^-\pi^0)\pi_s^+$  decay channel is shown. The black dots represent the data and the blue, dotted red and dotted blue lines represent the total fit, the signal and background components of the fit respectively.

91 signal yield is measured to be  $305 \pm 15$  per  $\text{fb}^{-1}$  of collected data. The uncertainty in the  
 92 measurement includes the statistical uncertainty and the uncertainty in the correction factor for  
 93 the peaking backgrounds which was measured using MC samples.

## 94 7 Tau mass measurement

95 Precise measurement of the properties of the tau lepton, in particular, its mass and lifetime, can  
 96 provide important tests of lepton flavor universality of SM. Currently, the relative precision of  
 97 these measurements for the tau lepton are nearly three orders of magnitude worse than those  
 98 for muon and electron. For the measurement of the mass of the tau lepton at Belle II<sup>9</sup>, the  
 99 tau-pair production events are selected by reconstructing events compatible with a 3-prong  
 100 ( $\tau^+ \rightarrow \pi^+\pi^-\pi^+\bar{\nu}_\tau$ ) and a 1-prong ( $\tau^- \rightarrow \ell^-\bar{\nu}_\ell\nu_\tau$ ,  $\tau^- \rightarrow h^-\nu_\tau$  or  $\tau^- \rightarrow \pi^-\pi^0\nu_\tau$ ) decay of the  
 101 tau pair.

102 To measure the tau mass, the pseudomass variable,  $M_{min}$ , is used which is defined in the  
 103 following way in order to have a kinematical edge at the tau mass:

$$M_{min} = \sqrt{M_{3\pi}^2 + 2(E_{\text{beam}} - E_{3\pi})(E_{3\pi} - P_{3\pi})} \leq m_\tau, \quad (3)$$

104 where,  $M_{3\pi}$ ,  $E_{3\pi}$ , and  $P_{3\pi}$ , are the mass, energy and momentum of the  $3\pi$  system and  $E_{\text{beam}}$   
 105 is the beam energy. An empirical edge function is used to extract the mass of the tau lepton  
 106 from the the kinematical end-point in the  $M_{min}$  distribution. The bias in the fit procedure is  
 107 estimated by using simulated samples with shifted values for the generated tau mass. Using  
 108  $8.8 \text{ fb}^{-1}$  of data, the tau mass is measured as:

$$\tau = 1777.28 \pm 0.75 \text{ (stat.)} \pm 0.33 \text{ (syst.) MeV} \quad (4)$$

109 Currently the precision of this measurement is limited by the size of the data that was used  
 110 and the systematical uncertainties due to corrections in the tracking and the fit bias. However,  
 111 as can be seen in left plot in Figure 5, the systematical uncertainties are already comparable to  
 112 those at Belle.

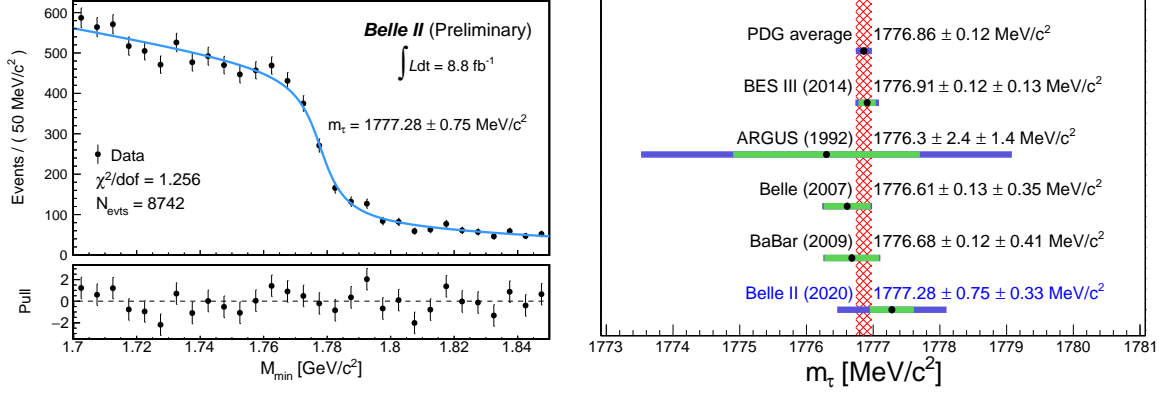


Figure 5 – Left plot shows the distribution of the data and the fit results on the  $M_{min}$  distribution and the extracted value for  $\tau$  and the corresponding statistical uncertainty after the fit bias correction. The right plot shows the comparison of the different  $\tau$  measurements, where the hashed red band shows the world average and the green and blue bars represent the systematic and statistical uncertainties respectively.

## 113 8 Summary

114 Thanks to the heroic efforts of the colleagues stationed in Tsukuba, the Belle II and SuperKEKB  
 115 have been performing persistently even through the difficult times caused by the current pan-  
 116 demic. Even though the size of the data collected so far is still a fraction of the ones at Belle  
 117 and BaBar, many Belle II analyses already have competitive systematic precisions and many of  
 118 the currently limiting systematic sources of uncertainties are expected to be reduced as larger  
 119 control samples are collected and the over understanding of the detector is improved.

## 120 References

- 121 1. K. Akai *et al.* (SuperKEKB), “SuperKEKB Collider,” Nucl. Instrum. Meth. A **907**  
 122 (2018), 188-199 doi:10.1016/j.nima.2018.08.017 [arXiv:1809.01958](#) [[physics.acc-ph](#)].
- 123 2. T. Abe *et al.* (Belle II Collaboration), “Belle II Technical Design Report,” [arXiv:1011.0352](#)
- 124 3. Belle II Collaboration, “Studies of the semileptonic  $\bar{B}^0 \rightarrow D^{*+} \ell^- \bar{\nu}_\ell$  and  $B^- \rightarrow D^0 \ell^- \bar{\nu}_\ell$   
 125 decay processes with  $34.6 \text{ fb}^{-1}$  of Belle II data,” [arXiv:2008.07198](#) [[hep-ex](#)]. [BELLE2-](#)  
 126 [CONF-PH-2020-008](#)
- 127 4. Belle II Collaboration, “Measurement of Hadronic Mass Moments  $\langle M_X^n \rangle$  in  $B \rightarrow X_c \ell \nu$   
 128 Decays at Belle II,” [arXiv:2009.04493](#) [[hep-ex](#)]. [BELLE2-CONF-PH-2020-011](#)
- 129 5. Belle II Collaboration, “Measurement of the time-integrated mixing probability  $\chi_d$  with a  
 130 semileptonic double-tagging strategy and  $34.6 \text{ fb}^{-1}$  of Belle II collision data”, [BELLE2-](#)  
 131 [CONF-PH-2021-004](#)
- 132 6. Belle II Collaboration, “Measurement of the branching fractions of  $B \rightarrow \eta' K$  decays using  
 133 2019/2020 Belle II data,” [BELLE2-CONF-PH-2021-007](#), [arXiv:2104.06224](#) [[hep-ex](#)]
- 134 7. Belle II Collaboration, “ $D^0$  Lifetime Plots with 2019 Data”, [BELLE2-NOTE-PL-2020-008](#)
- 135 8. Belle II Collaboration, “Preliminary analysis of  $D^{*+} \rightarrow D^0(\pi^+ \pi^- \pi^0) \pi^+$ ”, [BELLE2-](#)  
 136 [NOTE-PL-2021-003](#)
- 137 9. Belle II Collaboration, “ $\tau$  lepton mass measurement at Belle II”, [BELLE2-CONF-PH-2020-](#)  
 138 [010](#) [arXiv:2008.04665](#) [[hep-ex](#)]